

Optical Detection of Cancers

Xin-Hua Hu

Jun Qing Lu

Department of Physics, East Carolina University, Greenville, North Carolina, U.S.A.

INTRODUCTION

The American Cancer Society estimates that approximately 570,000 cancer deaths will occur in 2005 in United States.^[1] The key to achieving the desired patient prognosis is to detect cancer in the early stages. Among various diagnosis modalities, optical detection stands out for its potential of safety to patients and health professionals with nonionizing radiation, noninvasive nature of detection, high spatial resolution, and modest cost of equipment. Optical detection of cancers is a vast subject that has attracted intensive research efforts over the last few decades. It is therefore impossible to survey the field in a relative short essay like the current one. Instead, we will focus on the *in vivo* results that may lead to the noninvasive staging of dysplasia and cancers. Some *in vitro* data will be included here to reflect the historical development of a method or when *in vivo* results are not available.

It has been widely accepted that cancer originates from the accumulated mutation of DNA molecules within a cell or cells that tips the balance of cell cycle toward proliferation.^[2] Cancerous cells multiply without regulation to form a morphologically distinctive mass of tissue consisting of their clones in a local organ, often termed dysplasia, before the mass grows in size and eventually metastasizes into other organs to become a malignant tumor. Nearly all cancers develop in a staged fashion and the gold standard of cancer diagnosis and staging is the histopathologic analysis of biopsied tissues.^[3] Even with this very invasive and time-consuming technique, the criteria for staging of the dysplasia or the precancer stages are still not well defined and diagnosis varies significantly among pathologists. As a result, optical diagnosis of dysplasia lacks some clear standards to be validated against albeit greatly desired by physicians.

Optical detection of lesions was called “optical biopsy” in various publications in reference to the hope that a noninvasive replacement of biopsy and histopathology could be achieved optically. To reach this goal, one must identify the optical signatures of dysplasia and subsequent stages of cancer development, which may be correlated to three different types of variations: the mutation at the molecular level, the morphological variations at the cellular level, and

variations in tissue and vasculature (blood volume and oxygen saturation) structures at the tissue level. Optical detection of these changes at the three levels has been pursued with different regimes of measurements to acquire light signals from the ultraviolet to the infrared regions. These measurement regimes are sketched in Fig. 1 according to the wavelength relations between the excitation and the measured light signals. The following sections are divided on the basis of these relations.

THE RADIATIVE TRANSFER METHOD

Response of a biological system such as cells or tissues to an incident light field can be categorized into different types, as shown in Fig. 1. In the spectral region from about 300 to 2500 nm wavelength, elastic scattering of incident light by various components of tissues including the cells is often the dominant form of interaction. The measurement of optical signals as a result of elastic scattering and absorption is denoted here as the radiative transfer method because of the modeling methodology to be described below.

The light absorption and scattering can be understood fundamentally through the theory of classical electrodynamics in terms of the local fluctuation of the dielectric coefficient $\varepsilon(\mathbf{r}, \omega)$ or the related index of refraction $n(\mathbf{r}, \lambda_h) = [\varepsilon(\mathbf{r}, \omega)]^{1/2}$ at the scales of intracellular organisms, where \mathbf{r} is the position vector and $\lambda_h = 2\pi v/\omega$ is the wavelength, v and ω are the speed and angular frequency of incident light in the host medium, respectively. To demonstrate this point quantitatively, consider the scattering of an incident light field $(\mathbf{E}_i, \mathbf{B}_i)$ with a wave vector \mathbf{k}_i by a biological cell. The scattering configuration and the intracellular structure, given by $\varepsilon(\mathbf{r}, \lambda_h)$, are schematically presented in Fig. 2. Using Maxwell's equations, the scattered light field $(\mathbf{E}_s, \mathbf{B}_s)$ along the direction of the wave vector \mathbf{k} in the far-field region can be defined by an amplitude function $\mathbf{F}(\mathbf{k}, \mathbf{k}_0)$ as^[4]

$$\mathbf{E}_s(\mathbf{r}, \lambda_h) = \mathbf{F}(\mathbf{k}, \mathbf{k}_i) \frac{e^{jkr}}{r} \quad (1)$$

where \mathbf{k} and \mathbf{k}_i are related to the wavelength as $k = |\mathbf{k}| = |\mathbf{k}_i| = 2\pi/\lambda_h$. The amplitude function

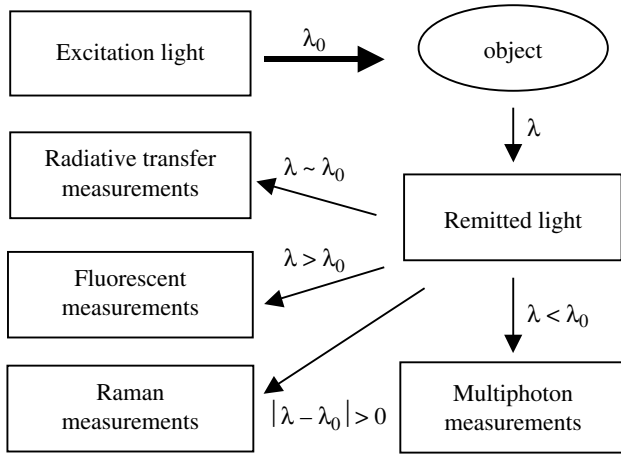


Fig. 1 Different approaches of optical measurements.

$\mathbf{F}(\mathbf{k}, \mathbf{k}_i)$ and the total field \mathbf{E} , the incident plus the scattered, are to be solved from the following equation:

$$\mathbf{F}(\mathbf{k}, \mathbf{k}_i) = \frac{1}{4\pi} \int_V (k^2 + \nabla \nabla \cdot) \times [\varepsilon(\mathbf{r}', \omega) - \varepsilon_h] \mathbf{E}(\mathbf{r}', \omega) e^{-j\mathbf{k} \cdot \mathbf{r}'} d^3 r' \quad (2)$$

where V is the cellular volume in which $\varepsilon - \varepsilon_h$ is a spatial function of \mathbf{r} . These relations show that light scattering is caused by the local inhomogeneity in terms of the deviation of the dielectric coefficient $\varepsilon(\mathbf{r}', \lambda)$ from the background value ε_h of the host medium. Further, light absorption can be accounted for by using a complex dielectric coefficient or complex refractive index $n = n_r + jn_i$, where $j = \sqrt{-1}$ and n_i causes attenuation of the incident wave in addition to scattering. Although analytical solutions can be obtained for scatterer of regular geometric shapes and structures, numerical solutions are the only feasible methods for scatterers of irregular but realistic shapes and inhomogeneous internal structures.

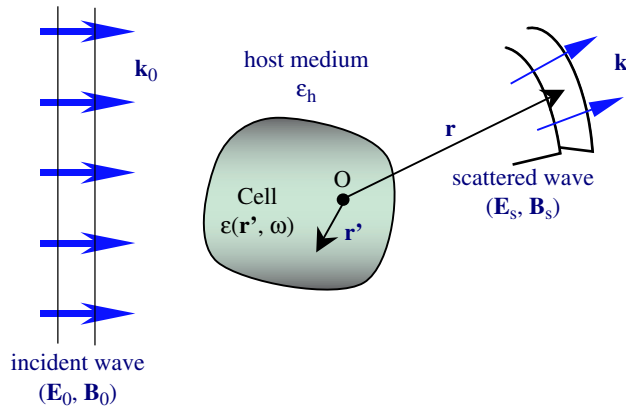


Fig. 2 Light scattering by a biological cell. (View this art in color at www.dekker.com.)

Biological tissues consist of many types of cells and extracellular components and usually possess no long-range orders or symmetry. The structural complexity of tissues renders the first-principle approach demonstrated in Eqs. (1) and (2) impractical. Even numerical solutions of tissue optics problems are impossible at the present time owing to the prohibitive computing cost. For modeling tissue optics problems, radiative transfer theory is a much preferred approach in which only the distribution of light radiance, $I(\mathbf{r}, \hat{s}, t)$, instead of the electromagnetic fields, is to be solved. The light radiance $I(\mathbf{r}, \hat{s}, t)$ is defined as the electromagnetic energy propagating along the \hat{s} direction per unit solid angle and per unit area at location \mathbf{r} and time t . The distribution of the radiance I can be obtained from a radiative transfer equation based on energy conservation:^[5]

$$\begin{aligned} \frac{1}{v} \frac{\partial I(\mathbf{r}, \hat{s}, t)}{\partial t} + \hat{s} \cdot \nabla I &= -(\mu_s + \mu_a) I(\mathbf{r}, \hat{s}, t) \\ &+ \mu_s \int_{4\pi} p(\hat{s}, \hat{s}') I(\mathbf{r}, \hat{s}', t) d\Omega' \\ &+ S(\mathbf{r}, \hat{s}, t) \end{aligned} \quad (3)$$

where \hat{s} is a unit vector of direction, μ_s and μ_a are the scattering and absorption coefficient, respectively, $p(\hat{s}, \hat{s}')$ is the scattering phase function, and S is the source term. In principle the optical parameters of tissue, μ_s , μ_a , and $p(\hat{s}, \hat{s}')$, can be derived from the scattering theory presented in Eq. (2) if the details of the optical inhomogeneity ε or n are completely known.^[6] It has recently been proved experimentally that the complex refractive index of microspheres, relative to the known refractive index of water as the host medium, can be determined accurately from optical measurements of the microsphere suspensions based on Eq. (3) and the Mie theory of light scattering by spheres.^[7] For complex turbid systems such as the biological tissues, it is nearly impossible to solve analytically the practical boundary problems described by Eq. (3). Instead, numerical solutions have to be resorted to and a statistical method of Monte Carlo simulation has been widely adopted for its algorithm simplicity and ease of implementation of the parallel computing technique.^[8,9]

If scattered light can be neglected or removed from the measured data using techniques such as spatial filtering, Eq. (3) can be solved for a source-free medium by simple integration to yield the modified Beer-Lambert law:

$$\frac{I(\mathbf{r}, \hat{s})}{I(\mathbf{r}_0, \hat{s})} = \exp \left\{ - \int_{\mathbf{r}_0}^{\mathbf{r}} \mu_t(\mathbf{r}') d\mathbf{r}' \right\} \quad (4)$$

where we define the attenuation coefficient $\mu_t = \mu_s + \mu_a$, neglect the second term on the right-hand side of Eq. (3) because it produced scattered light only, and consider only the steady-state solutions to drop the time variable. Eq. (4) yields a “shadowgram” principle to relate the projection image data in the transmission mode to the distribution of μ_t in the imaged object and forms the foundation for computed tomography (CT).^[10]

At the other extreme of approximation, the radiative transfer equation can be simplified to a diffusion equation of a “diffuse photon density wave,” represented by $\rho_d(\mathbf{r}, t) = \int_{4\pi} I_d(\mathbf{r}, \hat{\mathbf{s}}, t) d\Omega$, by considering only the portion of radiance that has been multiply scattered, i.e., I_d . Once the propagation directions of these photons are randomized by multiple scattering, the distribution of ρ_d is no longer related to the detailed form of the scattering process and depends only on the absorption coefficient μ_a and a reduced scattering coefficient $\mu_s' = \mu_s(1-g)$, where $g = \int_{4\pi} (\hat{\mathbf{s}} \cdot \hat{\mathbf{s}}') p(\hat{\mathbf{s}}, \hat{\mathbf{s}}') d\Omega'$ is the first moment of the scattering phase function. The diffusion approximation breaks down in two cases. The first case arises when μ_a becomes appreciable in comparison with μ_s because the multiply scattered portion I_d is significantly reduced by absorption and thus may not dominate in the light distribution I . The second case is in the region near a light source where most incident photons do not yet experience multiple scattering.

Continuous-Wave Imaging Studies

One of the earliest attempts to detect pathological conditions of tissues has been reported by Cutler, who observed projection images of breasts with visible light in the transmission mode in a dark room.^[11] Projection imaging of the breast or diaphanography has been actively studied in the 1970s and 1980s by using both visible and near-infrared light sources with films or video cameras as the recording devices.^[12] These studies employed the shadowgram principle for image interpretation and often were compared with x-ray mammography.^[13] Unlike the case of x-rays in which the photons that undergo volumetric trajectories due to scattering can be effectively removed from the projection data, light scattering dominates over absorption in interaction of the visible or near-infrared photons with the breast tissues. Consequently, blurring is inherent in the optical projection images. Both contrast and spatial resolution of these images, for discriminating different types of breast tissues and lesions, have been shown to be poor in comparison with x-ray mammography and research interest has diminished.

For organs other than breast, transillumination imaging is not practical and imaging in the reflection

mode is the only way to measure the optical response from tissues noninvasively. Several low-magnification microscopes or endoscopes have been routinely used in clinics by physicians as the cancer screening tools to enhance their ability of visual inspection. These include dermoscopy in detection of skin cancers, colposcopy in cervical cancers, colonoscopy in colon cancers, and bronchoscopy in lung and airway cancers. Recently, multispectral imaging has been investigated for early diagnosis of dysplastic nevi and melanoma.^[14] Quantitative modeling of the projection data in the reflection mode to obtain tomographic images, however, is extremely difficult because these signals originate from the refractive index mismatch at the tissue surface and scattered photons in the bulk tissue. Researchers have followed two directions: 1) to extract patterns and statistical features from image data and/or spectroscopy data to correlate with the pathology for cancer detection and 2) to determine the local tissue optical parameters from multipoint measurements of the reflectance with a tissue optics model. These will be discussed in this and the following sections. Elbaum et al. acquired in vivo images from 246 pigmented skin lesions, ranging from benign nevi to dysplasia to melanoma, with 10 wavebands between 430 and 950 nm using a dermoscope.^[15] The multispectral images were processed with different algorithms of patterns analysis to extract about 25 image parameters in two groups. Comparison of the two-parameter groups as classifiers with the histopathology analysis demonstrated good sensitivity (100% or 95%) and relatively poor specificity (84% or 68%). A similar in vivo method for melanoma diagnosis has been investigated on 237 pigmented skin lesions and 80% sensitivity and 51% specificity (with lesion dimension considered) were reported.^[16]

Spectroscopy Measurements

For noninvasive in vivo detection of cancer, reflectance spectroscopy with a continuous-wave (cw) white light source has been the preferred mode of measurements by researchers for its instrumental simplicity. A technique of spatially resolved diffuse reflectance has been introduced to determine μ_a and μ_s' from the spatial dependence of reflectance signals. The spatially resolved signals are acquired with multiple fibers and fitted to calculated curves based on a diffusion model of a homogenous tissue.^[17] The wavelength dependence of the parameters μ_a and μ_s' can be obtained from the spectroscopy data to analyze the chromophores in the tissue. But clinical application of this spatially resolved technique is limited because the homogeneity should not be assumed in tissues with cancerous regions. As a result, published in vivo

spectroscopy studies up to this time have combined only the single-point detection with pattern analysis of data based on various statistical methods. Improvement in modeling accuracy with Monte Carlo simulations has been reported.^[18]

Mirabal et al. investigated reflectance spectroscopy in the regions from 390 to 590 nm and from 350 to 650 nm to evaluate its potential for diagnosis of cervical tissue conditions in patients with abnormal Pap smears.^[19,20] They analyzed the spectral data statistically to extract classifiers for correlating with pathological diagnosis and compared the correlation with that determined with 355 nm-excited fluorescence spectroscopy measurements. It was concluded that fluorescence spectroscopy provided better specificity and sensitivity in the detection of cervical intraepithelial neoplasia.^[19] In vivo measurements of the reflectance spectral data and statistical analysis have been performed in an attempt to detect breast cancers, lesions in ovarian tissues, skin lesions including dysplastic nevi and basal cell carcinomas, and adenomatous colon polyps.^[21–24] Recently, Johnson et al. reported the study of spectral reflectance data, between 340 and 900 nm, acquired from 139 cancerous and normal sentinel nodes removed from 68 patients with breast cancers.^[25] Statistical analysis of the spectral data yielded scores for discriminating different types of nodes with sensitivity and specificity comparable to those of frozen section histology.

In the above studies, the measured light signals included those photons that are scattered only once or a few times in the backward directions and others that are scattered multiple times. Detection of singly backscattered photons can be realized experimentally with a single fiber of small diameter of about 200 μm for both launch and detection of light. Because multiply scattered photons in the remitted light are most likely to migrate away from the fiber, the detected signal is dominated by singly backscattered photons from the superficial layer of the tissue.^[26] Georgakoudi et al. compared three types of in vivo spectral data to evaluate their potentials for detection of dysplasia in 16 patients with Barrett's esophagus: singly backscattered light; diffuse reflectance; and intrinsic fluorescence of multiple excitation wavelengths. It was found that singly backscattered light spectroscopy data provided the best overall sensitivity and specificity among the three techniques in separating different degrees of dysplasia.^[27]

Frequency-Domain Measurements

Intensity modulation of a cw laser beam at a megahertz frequency adds "signatures" to the beam in terms of amplitude demodulation M and phase shift

ϕ . When such a beam is launched into tissue, the local optical properties of the tissue cause variation in M and ϕ in the detected signals relative to the source. With a diffusion model, M and ϕ can be inverted to obtain tissue's optical parameters μ_a and μ_s' at selected wavelengths if multiple laser sources are used.^[28] Further, several fibers can be employed to launch and measure at different locations to reconstruct tomographic images with contrast built on M , ϕ , their spatial derivatives, or μ_a and μ_s' . An early study of one breast cancer patient using the frequency-domain method at 690 and 825 nm was reported by Fantini et al., who also determined μ_a and μ_s' for normal and tumor tissues.^[29] Their very limited in vivo result suggested that μ_a and μ_s' of tumor tissues are both larger than those of the normal tissues at both wavelengths. A similar method has been used to determine μ_a and μ_s' at the sites of lesions and normal tissues on one patient with lung carcinoma and subcutaneous tumors and 10 patients with cervical carcinoma in situ at four wavelengths from 674 to 956 nm.^[30,31] The results, however, exhibited significant overlap in the values of these parameters between the normal tissue sites and lesion sites at the four wavelengths. The frequency-domain method can be further improved to enhance the image contrast of the blood oxygenation by incorporating a spatial derivative algorithm.^[32] This technique was used for an in vivo study conducted on four patients with ductal carcinomas and fibroadenoma in their breasts. Transmission images were obtained at four wavelengths by scanning the source and detection fibers in tandem and image data yielded evidence of a correlation between the lesion locations, identified by x-ray mammography and histopathology, and those of abnormality in the oxygenation index images.^[32]

Time-Resolved Measurements

The significant blurring in the cw imaging data due to the dominant presence of multiply scattered light causes substantial deterioration in the contrast of images interpreted through the shadowgram principle. As ultrashort pulsed solid-state lasers and fast photodetectors became routinely available, research interest in shadowgram imaging for cancer detection has been revived since the early 1990s. Various time-gating methods have been devised to extract the early-arrival photons, which are either not scattered (ballistic photons) or only weakly scattered (snake photons).^[33] Optical parameters μ_a and μ_s' can be obtained with a diffusion model or Monte Carlo method from the time-resolved signals of reflectance or transmittance at the wavelength of excitation.^[34,35] An in vitro study of 20 excised breast samples consisting of either fat (lipid) or fibrous tissues with a streak camera of 2 psec

time resolution has shown that the mean value of μ_s' is about 0.5 mm^{-1} for lipid tissue and 0.9 mm^{-1} for fibrous tissue at the wavelength of 800 nm.^[36] Patients with breast cysts or tumors have been studied with the time-resolved technique to obtain transmission images by scanning the source fibers connected to a diode laser generating 400 psec pulses and a photomultiplier detector on the opposite side of the compressed breast.^[37,38] Even though lesions or tumors of a few centimeters in size can be identified from the images, with the prior knowledge from MRI and x-ray mammography, no significant reduction in blurring can be observed in the time-resolved images when compared with the cw images, which may be attributed to the low time resolution of the above optical systems.^[12]

Diffuse Optical Tomography

Unlike its x-ray counterpart, optical tomography remains an open problem despite intensive research efforts. The complexity of the problem arises from the fact that the measured light signals from a turbid object are dominated by photons with volumetric trajectories in the imaged region as a result of light scattering. Inverse algorithms for reconstructing 2D images of optical parameters from the projections have been investigated in phantoms with simple-shaped structures embedded. The existence of unique solutions in practical cases, however, is unknown.^[39] Most published studies on optical tomography employed the method of fiber-based multipoint detection in the frequency domain to obtain measured data, instead of the cw or time-resolved techniques, for instrumental simplicity and large dynamic range. In diffuse optical tomography (DOT), the diffusion model is used for forward calculations of the measured data from trial values of optical parameters based on simplified models of tissue heterogeneity. Even though DOT possesses the ability to exhibit the distribution of blood oxygen saturation in tissues, fast and robust inverse algorithms for image reconstruction remain to be developed. Existing inverse algorithms for DOT are iterative processes of least-squares type or of Bayesian type using an objective function and their solutions are practical only if the number of unknown optical parameters is kept small by either using a priori structural information as constraints or reducing the number of voxels (or spatial resolution).^[40] Consequently, recent research efforts have been concentrated on the development of DOT as an auxiliary modality to other high-resolution imaging modalities such as x-ray CT or MRI to enhance the functional imaging capacity.^[41] A preliminary in vivo study of a breast tumor with DOT demonstrated the overlapping of the abnormal

locations in the images of μ_a and μ_s' at multiple wavelengths with the biopsy identified tumor site.^[42]

Optical Coherence Tomography

Reconstruction of tomographic images of an object in optical coherence tomography (OCT) is accomplished in reflection mode by combining the single-point measurement using a converging light beam of broad spectral bandwidth with 2D or 3D scanning. The OCT signal is based on the light backscattered from the focal point and is separated from the background noise by interference of the signal beam with a reference beam. High spatial resolution can be achieved in the longitudinal (depth) direction, ranging from 2 to $20 \mu\text{m}$, using a light source of short coherent length.^[43] The resolutions in the transverse directions relate to both the imaging optics and the size of the scanning step. The OCT image contrast depends on two factors: the attenuation of the incident beam along its trajectory toward the focal point and the local gradient of the refractive index at the focal point. As a result, OCT signals are attenuated exponentially as $\exp\{-2 \int_0^d \mu_t dr\}$ within the interrogated tissue, where d is the pathlength from tissue surface to the focal point.

Optical coherence tomography has been employed successfully for detection of intraocular tumors because μ_t for most ocular tissues is much less than 1 mm^{-1} in the visible and near-infrared regions.^[44] For turbid biological tissues such as the human skin and mucosa, μ_t typically ranges from 1 to 10 mm^{-1} and the penetration depth of OCT in these tissues is limited to about 1 mm or less.^[45] The small penetration depth in turbid tissues is the major factor limiting the application of OCT for cancer detection. In a recent study, two patients with diagnosis of invasive basal cell carcinoma in their skin have been imaged with a polarization sensitive OCT method to identify structural changes in the superficial layers of the sites.^[46] The OCT images showed variations in both tumor sites, which were attributed to the local changes in the refractive index due to the loss of normal tissue structure by the invasive growth of dense tumor stroma. An in vivo study of OCT in the detection of oral tumors has been conducted in an animal model of 35 hamsters with squamous cell carcinoma and it was found that in 80% of cases the OCT-based diagnosis correlates with those based on histopathology.^[47]

Optical coherence tomography can also be implemented in the endoscopic form for in vivo imaging of luminal cancers by passing a catheter-based fiber probe through the biopsy channel of an endoscope.^[48,49] Examination of upper gastrointestinal tracts has been

performed with endoscopic OCT in 32 patients suspected of Barrett's esophagus and esophageal adenocarcinoma, followed by the endoscopic mucosal biopsies.^[50] The OCT images were compared to the histopathology analysis of the biopsied tissues and it has been found that OCT images provide sufficient contrast to differentiate among the normal esophagus, Barrett's esophagus, and esophageal adenocarcinoma. A similar *in vivo* study of 19 patients with Barrett's esophagus and esophageal adenocarcinoma confirmed that the abnormal morphologic changes in the mucosa tissues can be identified from the OCT images.^[51]

THE FLUORESCENCE METHOD

Fluorescence signals from biological macromolecules depend on the structure of electronically excited states of these molecules. This relation allows the possibility to discriminate molecules in cancerous cells or tissues from those in the normal counterparts. The strong signals, assuming the existence of either intrinsic or extrinsic fluorophores, and the ability for molecular imaging or detection have made the fluorescence method a popular approach to probe biological systems. These advantages, however, can be significantly reduced owing to the overlapping of spectral features in the broadband fluorescence spectra from different biological fluorophores and the dependence of the spectral shape on the tissue optical parameters resulting from the transport of fluorescence light in the interrogated tissues. This typically leads to poor specificity as the barrier for cancer detection in clinical settings. Future research efforts have to be invested for translation of the fluorescence method into clinical applications with much improved signal-to-noise ratios. We review here only the measurements of fluorescence signals emitted by intrinsic fluorophores, which is also called autofluorescence.

Spectroscopy Measurements

Measurements of fluorescence signals are usually carried out with cw excitation at wavelengths λ_0 in the ultraviolet and blue regions because of large absorption cross sections and often, high-fluorescence quantum yields. The distinctive features of cw fluorescence signals are given by the excitation and emission spectra and associated quantum yields or signal intensities.

Alfano et al. compared the difference in fluorescence spectra by intrinsic fluorophores of normal and tumor tissues of animals and humans.^[52,53] The fluorescence spectra were obtained with an argon laser beam at 488 nm and power of up to 100 mW focused on a spot of about 0.1 mm in diameter. These fluorescence

spectra were shown to be dominated by a broadly peaked curve in the wavelength range from 500 to 650 nm with no significant structure. It has been suggested that the signal differences at selected wavelengths in the emission spectra between tissues pathologically classified as normal and cancerous may provide the means for cancer detection.^[52,53] These early spectral measurements did not provide sufficient evidences, however, for cancer detection because the contrast or signal-to-noise ratio was small and sample-to-sample fluctuation was not considered. Additional studies of fluorescence with ultraviolet excitation from 300 to 460 nm on breast tissues provided statistically significant results, which demonstrated that spectral features are very similar among the normal and tumor tissues but the fluorophore concentration and/or fluorescence efficiency may differ in certain spectral regions.^[54,55] Even though these researchers reported that features of emission spectra can be utilized in the form of ratios of fluorescence signals at two wavelengths to differentiate cancerous tissues from the normal breast tissues, the spectra presented in these results vary from each other with no explanation provided. The technique of fluorescence emission ratio has been used for *in vivo* investigation of bronchial tissues with excitation between 350 and 495 nm. After correcting the effects of probe-tissue distance and intensity variation of excitation, it has been found that the normal bronchial tissue exhibits slightly stronger emission than the dysplasia tissue with nearly identical spectral shapes, while those of the cancerous ones were much weaker than both tissues.^[56] Similar *in vivo* study of emission ratio differences has also been reported for distinguishing nasopharyngeal carcinoma and normal tissue.^[57]

The similarity in the shapes of emission spectra between the normal and cancerous tissues significantly reduces the reliability of this technique for cancer detection. Several methods have been investigated to address this problem by either statistical analysis of spectral data to decrease the noise or employment of multiwavelength excitation to increase the signal content. Multivariate analysis methods based on principal component analysis (PCA) and support vector machines were introduced to identify spectral features that can be correlated to the pathology condition of tissues.^[58,59] A method of excitation-emission matrix (EEM) with multiple excitation wavelengths was applied to colonic mucosa tissue analysis.^[60] For over 10 yr, a research group led by Richards-Kortum has studied the fluorescence detection of cervical cancer with methods of both EEM and PCA.^[61,62] Brewer et al. collected the *in vivo* emission spectra of ovarian tissues with 18 excitation wavelengths from 330 to 500 nm from patients suspected to have ovarian cancers.^[63] On the basis of EEM analysis, it has been

suggested that certain spectral patterns in EEM plots may be correlated to the pathological conditions of the ovarian tissues for cancer detection.

Time-Resolved Measurements

One valuable method to differentiate molecules with overlapping spectra and/or reduce the effect of tissue optical parameters on the spectral shapes of fluorescence signals is to determine the relaxation times of fluorescence signals with a time-resolved technique. Time-resolved measurements probe directly the relaxation of electronically excited fluorophores back to their ground state in the time domain. Typical lifetimes of transitions between the singlet excited and ground states are 1–10 nsec. Hence, subnanosecond light pulses from pulsed lasers such as nitrogen lasers are required for excitation and detectors with similar time resolution must be used. Single- or multi-component fitting with exponential decay curves can be used to extract relaxation times from the fluorescence data. An *in vitro* study of 18 normal, benign, and malignant human breast tissues has been performed with excitation at 310 nm and emission at 340 nm.^[33] By fitting the measured data with two-component exponential curves, a large difference was found in the ratio of the two decay components among the samples: the malignant tumor tissues have the largest portion of the slow component (with relaxation time about 2 nsec) among the three types. A similar assessment of fixed but unstained breast tissues from six patients with benign or malignancy-associated collagenous stroma has been recently reported with a fluorescence lifetime imaging system of 2 nsec time resolution and excitation at 415 nm.^[64] A seemingly opposite trend, however, has been observed in the above study: pixels of benign stroma show larger relaxation times than those of malignancy-associated stroma. Further studies are obviously needed.

OTHER METHODS

Owing to the limitation of space, we have to exclude certain optical methods from discussion, which nevertheless have the potential for cancer detection. Among these, three are briefly presented here: confocal microscopy, Raman spectroscopy, and multiphoton techniques. Confocal microscopes have become a standard imaging tool in biology laboratories since the early 1990s for reconstruction of 3D images of cells and other microscopic agents. Its optical principle is similar to that of OCT except for the collection of backscattered light through spatial filtering with a microscopic objective of large numerical aperture. Confocal images of turbid tissues typically exhibit contrasts superior to

the OCT images.^[65] *In vivo* applications of confocal imaging in clinics have been investigated mostly in dermatology for the detection of skin structures and lesions.^[66] In comparison with the very active research on radiative transfer and fluorescence methods, the study of Raman spectroscopy and multiphoton techniques received relatively less attention for *in vivo* optical detection of cancers in tissues. The major challenge relates to the detection of weak signals, which requires intense light sources and sensitive detectors. Lasers are necessary to meet the requirement of high irradiance for nonlinear measurements and both high irradiance and narrow frequency bandwidth for Raman measurements. These methods have been studied for cancer detection with Raman spectroscopy and multiphoton microscopy and for analysis of the skin dermis by the second-harmonic signals.^[67–69]

CONCLUSIONS

Compared with established diagnosis modalities, such as x-ray, CT, and MRI, noninvasive optical detection of cancers has been regarded to have considerable advantages, which include patient safety, high spatial resolution, and low equipment cost. These advantages have attracted intensive research efforts over the last two decades and substantial strides have been made toward modeling of light–tissue interactions and instrumentation development for data acquisition. Despite this progress, optical detection of cancers has not yet achieved the status of the established imaging modalities. The fundamental barrier impeding the translation of optical technology from the laboratory to wide applications in clinics, in our view, relates to the lack of efficient modeling tools and algorithms to invert the measured data from turbid human tissues to the spatial distribution of optical parameters that is inherently heterogenous at the scale of millimeters or lower. It is, therefore, hoped that this barrier can be significantly reduced in the near future with interdisciplinary efforts contributed by researchers from multiple fields including the biomedical, computational, engineering, and physical sciences.

ACKNOWLEDGMENT

We acknowledge the partial support from the National Institutes of Health through a grant (1R15GM70798-01).

REFERENCES

1. ACS. Cancer Facts & Figures 2005. American Cancer Society, 2005.

2. Lodish, H.F.; Berk, A.; Matsudaira, P.; Kaiser, C.A.; Krieger, M.; Scott, M.P.; Zipursky, S.L.; Darnell, J. *Molecular Cell Biology*; 5th Ed.; W.H. Freeman and Company: New York, 2003.
3. Cotran, R.S.; Kumar, V.; Collins, T.; Robbins, S.L. *Robbins' Pathologic Basis of Disease*; 6th Ed.; Saunders: Philadelphia, 1999.
4. Lu, J.Q.; Yang, P.; Hu, X.H. Simulations of light scattering from a biconcave red blood cell using the FDTD method. *J. Biomed. Opt.* **2005**, *10* (2) 024022.
5. Chandrasekhar, S. *Radiative Transfer*; Dover Publications: New York, 1960.
6. van de Hulst, H.C. *Light Scattering by Small Particles*; Wiley: New York, 1957.
7. Ma, X.; Lu, J.Q.; Brock, R.S.; Jacobs, K.M.; Yang, P.; Hu, X.H. Determination of complex refractive index of polystyrene microspheres from 370 to 1610 nm. *Phys. Med. Biol.* **2003**, *48*, 4165–4172.
8. Wilson, B.C.; Adam, G. A Monte Carlo model for the absorption and flux distributions of light in tissue. *Med. Phys.* **1983**, *10* (6), 824–830.
9. Li, K.; Lu, J.Q.; Brock, R.S.; Yang, B.; Hu, X.H. Quantitative modeling of skin images using parallel Monte Carlo methods. *SPIE Proc.* **2005**, *5693*, 82–87.
10. Kak, A.C.; Slaney, M. *Principles of Computerized Tomographic Imaging*; IEEE Press: New York, 1988.
11. Cutler, M. Transillumination as an aid in the diagnosis of breast lesions. *Surg. Gynecol. Obstet.* **1929**, *48* (6), 721–729.
12. D'Orsi, C.J.; Bartrum, R.J.; Moskowitz, M.M. Light scanning of the breast. In *Mammography, Thermography, and Ultrasound in Breast Cancer Detection*; 2nd Ed.; Gold, R.H., Ed.; Grune & Stratton: New York, 1987; 169–177.
13. Profio, A.E.; Navarro, G.A.; Sartorius, O.W. Scientific basis of breast diaphanography. *Med. Phys.* **1989**, *16* (1), 60–65.
14. Moncrieff, M.; Cotton, S.; Claridge, E.; Hall, P. Spectrophotometric intracutaneous analysis: a new technique for imaging pigmented skin lesions. *Br. J. Dermatol.* **2002**, *146* (3), 448–457.
15. Elbaum, M.; Kopf, A.W.; Rabinovitz, H.S.; Langley, R.G.; Kamino, H.; Mihm, M.C., Jr.; Sober, A.J.; Peck, G.L.; Bogdan, A.; Gutkowitz-Krusin, D.; Greenebaum, M.; Keem, S.; Oliviero, M.; Wang, S. Automatic differentiation of melanoma from melanocytic nevi with multispectral digital dermoscopy: a feasibility study. *J. Am. Acad. Dermatol.* **2001**, *44* (2), 207–218.
16. Farina, B.; Bartoli, C.; Bono, A.; Colombo, A.; Lualdi, M.; Tragni, G.; Marchesini, R. Multi-spectral imaging approach in the diagnosis of cutaneous melanoma: potentiality and limits. *Phys. Med.* **2000**, *45* (5), 1243–1254.
17. Kienle, A.; Lilge, L.; Patterson, M.S.; Hibst, R.; Steiner, R.; Wilson, B.C. Spatially resolved absolute diffuse reflectance measurements for non-invasive determination of the optical scattering and absorption coefficients of biological tissue. *Appl. Opt.* **1996**, *35*, 2304–2314.
18. Pfefer, T.J.; Matchette, L.S.; Bennett, C.L.; Gall, J.A.; Wilke, J.N.; Durkin, A.J.; Ediger, M.N. Reflectance-based determination of optical properties in highly attenuating tissue. *J. Biomed. Opt.* **2003**, *8* (2), 206–215.
19. Nordstrom, R.J.; Burke, L.; Niloff, J.M.; Myrtle, J.F. Identification of cervical intraepithelial neoplasia (CIN) using UV-excited fluorescence and diffuse-reflectance tissue spectroscopy. *Lasers Surg. Med.* **2001**, *29* (2), 118–127.
20. Mirabal, Y.N.; Chang, S.K.; Atkinson, E.N.; Malpica, A.; Follen, M.; Richards-Kortum, R. Reflectance spectroscopy for in vivo detection of cervical precancer. *J. Biomed. Opt.* **2002**, *7* (4), 587–594.
21. Bigio, I.J.; Bown, S.G.; Briggs, G.; Kelley, C.; Lakhani, S.; Pickard, D.; Ripley, P.M.; Rose, I.G.; Saunders, C. Diagnosis of breast cancer using elastic-scattering spectroscopy: preliminary clinical results. *J. Biomed. Opt.* **2000**, *5* (2), 221–228.
22. Utzinger, U.; Brewer, M.; Silva, E.; Gershenson, D.; Blast, R.C., Jr.; Follen, M.; Richards-Kortum, R. Reflectance spectroscopy for in vivo characterization of ovarian tissue. *Lasers Surg. Med.* **2001**, *28* (1), 56–66.
23. Garcia-Urbe, A.; Kehtarnavaz, N.; Marquez, G.; Prieto, V.; Duvic, M.; Wang, L.V. Skin cancer detection by spectroscopic oblique-incidence reflectometry: classification and physiological origins. *Appl. Opt.* **2004**, *43*, 2643–2650.
24. Zonios, G.; Perelman, L.T.; Backman, V.; Manoharan, R.; Fitzmaurice, M.; Van Dam, J.; Feld, M.S. Diffuse reflectance spectroscopy of human adenomatous colon polyps in vivo. *Appl. Opt.* **1999**, *38* (31), 6628–6637.
25. Johnson, K.S.; Chicken, D.W.; Pickard, D.C.; Lee, A.C.; Briggs, G.; Falzon, M.; Bigio, I.J.; Keshtgar, M.R.; Bown, S.G. Elastic scattering spectroscopy for intraoperative determination of sentinel lymph node status in the breast. *J. Biomed. Opt.* **2004**, *9* (6), 1122–1128.
26. Canpolat, M.; Mourant, J.R. Particle size analysis of turbid media with a single optical fiber in contact with the medium to deliver and detect white light. *Appl. Opt.* **2001**, *40* (22), 3792–3799.
27. Georgakoudi, I.; Jacobson, B.C.; Van Dam, J.; Backman, V.; Wallace, M.B.; Muller, M.G.;

- Zhang, Q.; Badizadegan, K.; Sun, D.; Thomas, G.A.; Perelman, L.T.; Feld, M.S. Fluorescence, reflectance, and light-scattering spectroscopy for evaluating dysplasia in patients with Barrett's esophagus. *Gastroenterology* **2001**, *120* (7), 1620–1629.
28. Madsen, S.J.; Anderson, E.R.; Haskell, R.C.; Tromberg, B. Portable, high-bandwidth frequency-domain photon migration instrument for tissue spectroscopy. *Opt. Lett.* **1994**, *19* (23), 1934–1936.
29. Fantini, S.; Walker, S.A.; Franceschini, M.A.; Kaschke, M.; Schlag, P.M.; Moesta, K.T. Assessment of the size, position, and optical properties of breast tumors in vivo by noninvasive optical methods. *Appl. Opt.* **1998**, *37* (10), 1982–1989.
30. Fishkin, J.B.; Coquoz, O.; Anderson, E.R.; Brenner, M.; Tromberg, B.J. Frequency-domain photon migration measurements of normal and malignant tissue optical properties in a human subject. *Appl. Opt.* **1997**, *36* (31), 10–20.
31. Hornung, R.; Pham, T.H.; Keefe, K.A.; Berns, M.W.; Tadir, Y.; Tromberg, B.J. Quantitative near-infrared spectroscopy of cervical dysplasia in vivo. *Hum. Reprod.* **1999**, *14* (11), 2908–2916.
32. Heffer, E.; Pera, V.; Schutz, O.; Siebold, H.; Fantini, S. Near-infrared imaging of the human breast: complementing hemoglobin concentration maps with oxygenation images. *J. Biomed. Opt.* **2004**, *9* (6), 1152–1160.
33. Das, B.B.; Liu, F.; Alfano, R.R. Time-resolved fluorescence and photon migration studies in biomedical and model random media. *Rep. Prog. Phys.* **1997**, *60*, 227–292.
34. Patterson, M.S.; Chance, B.; Wilson, B.C. Time resolved reflectance and transmittance for the noninvasive measurement of tissue optical properties. *Appl. Opt.* **1989**, *28* (12), 2331–2336.
35. Kienle, A.; Patterson, M.S. Determination of the optical properties of turbid media from a single Monte Carlo simulation. *Phys. Med. Biol.* **1996**, *41*, 2221–2227.
36. Zacharakis, G.; Zolindaki, A.; Sakkalis, V.; Filippidis, G.; Papazoglou, T.G.; Tsiftsis, D.D.; Koumantakis, E. In vitro optical characterization and discrimination of female breast tissue during near infrared femtosecond laser pulses propagation. *J. Biomed. Opt.* **2001**, *6* (4), 446–449.
37. Torricelli, A.; Spinelli, L.; Pifferi, A.; Taroni, P.; Cubeddu, R. Use of a nonlinear perturbation approach for in vivo breast lesion characterization by multiwavelength time-resolved optical mammography. *Opt. Exp.* **2003**, *11* (8), 853–867.
38. Grosenick, D.; Wabnitz, H.; Moesta, K.T.; Mucke, J.; Moller, M.; Stroszcynski, C.; Stossel, J.; Wassermann, B.; Schlag, P.M.; Rinneberg, H. Concentration and oxygen saturation of haemoglobin of 50 breast tumours determined by time-domain optical mammography. *Phys. Med. Biol.* **2004**, *49* (7), 1165–1181.
39. Arridge, S.R. Optical tomography in medical imaging. *Inverse Problems* **1999**, *15*, R41–R93.
40. Arridge, S.R.; Hebden, J.C. Optical imaging in medicine: II. Modelling and reconstruction. *Phys. Med. Biol.* **1997**, *42* (5), 841–853.
41. Li, A.; Miller, E.L.; Kilmer, M.E.; Brukilacchio, T.J.; Chaves, T.; Stott, J.; Zhang, Q.; Wu, T.; Chorlton, M.; Moore, R.H.; Kopans, D.B.; Boas, D.A. Tomographic optical breast imaging guided by three-dimensional mammography. *Appl. Opt.* **2003**, *42* (25), 5181–5190.
42. Dehghani, H.; Pogue, B.W.; Poplack, S.P.; Paulsen, K.D. Multiwavelength three-dimensional near-infrared tomography of the breast: initial simulation, phantom, and clinical results. *Appl. Opt.* **2003**, *42* (1), 135–145.
43. Huang, D.; Swanson, E.A.; Lin, C.P.; Schuman, J.S.; Stinson, W.G.; Chang, W.; Hee, M.R.; Flotte, T.; Gregory, K.; Puliafito, C.A., et al. Optical coherence tomography. *Science* **1991**, *254* (5035), 1178–1181.
44. Shields, C.L.; Mashayekhi, A.; Luo, C.K.; Materin, M.A.; Shields, J.A. Optical coherence tomography in children: analysis of 44 eyes with intraocular tumors and simulating conditions. *J. Pediatr. Ophthalmol. Strabismus* **2004**, *41* (6), 338–344.
45. Knuttel, A.; Boehlau-Godau, M. Spatially confined and temporally resolved refractive index and scattering evaluation in human skin performed with optical coherence tomography. *J. Biomed. Opt.* **2000**, *5* (1), 83–92.
46. Strasswimmer, J.; Pierce, M.C.; Park, B.H.; Neel, V.; de Boer, J.F. Polarization-sensitive optical coherence tomography of invasive basal cell carcinoma. *J. Biomed. Opt.* **2004**, *9* (2), 292–298.
47. Wilder-Smith, P.; Jung, W.G.; Brenner, M.; Osann, K.; Beydoun, H.; Messadi, D.; Chen, Z. In vivo optical coherence tomography for the diagnosis of oral malignancy. *Lasers Surg. Med.* **2004**, *35* (4), 269–275.
48. Sergeev, A.M.; Gelikonov, V.M.; Gelikonov, G.V.; Feldchtein, F.I.; Kuranov, R.V.; Gladkova, N.D.; Shakhova, N.M.; Snopova, L.B.; Shakhov, A.V.; Kuznetzova, I.A.; Denisenko, A.N.; Pochinko, V.V.; Chumakov, Y.P.; Streltsova, O.S. In vivo endoscopic OCT imaging of pre-cancer and cancer states of human mucosa. *Opt. Exp.* **1997**, *1* (13), 432–440.
49. Ponomarev, J.M.; Nishioka, N.S. Diagnosis of Barrett's esophagus using optical coherence

- tomography. *Gastrointest. Endosc. Clin. N. Am.* **2003**, *13* (2), 309–323.
50. Bouma, B.E.; Tearney, G.J.; Compton, C.C.; Nishioka, N.S. High-resolution imaging of the human esophagus and stomach in vivo using optical coherence tomography. *Gastrointest. Endosc.* **2000**, *51* (4 pt 1), 467–474.
 51. Jackle, S.; Gladkova, N.; Feldchtein, F.; Terentieva, A.; Brand, B.; Gelikonov, G.; Gelikonov, V.; Sergeev, A.; Fritscher-Ravens, A.; Freund, J.; Seitz, U.; Schroder, S.; Soehendra, N. In vivo endoscopic optical coherence tomography of esophagitis, Barrett's esophagus, and adenocarcinoma of the esophagus. *Endoscopy* **2000**, *32* (10), 750–755.
 52. Alfano, R.R.; Tata, D.B.; Cordero, J.; Tomashefsky, P.; Longo, F.W.; Alfano, M.A. Laser induced fluorescence spectroscopy from native cancerous and normal tissue. *IEEE J. Quantum Electron.* **1984**, *20* (12), 1507–1511.
 53. Alfano, R.R.; Tang, G.C.; Pradhan, A.; Lam, W.; Choy, D.S.J.; Opher, E. Fluorescence spectra from cancerous and normal human breast and lung tissues. *IEEE J. Quantum Electron.* **1987**, *23* (10), 1806–1811.
 54. Gupta, P.K.; Majumder, S.K.; Uppal, A. Breast cancer diagnosis using N₂ laser excited autofluorescence spectroscopy. *Lasers Surg. Med.* **1997**, *21* (5), 417–422.
 55. Hage, R.; de la Riviere, A.B.; Seldenrijk, C.A.; van den Bosch, J.M. Update in pulmonary carcinoma tumors: a review article. *Ann. Surg. Oncol.* **2003**, *10* (6), 697–704.
 56. Zellweger, M.; Goujon, D.; Conde, R.; Forrer, M.; van den Bergh, H.; Wagnieres, G. Absolute autofluorescence spectra of human healthy, metaplastic, and early cancerous bronchial tissue in vivo. *Appl. Opt.* **2001**, *40* (22), 3784–3791.
 57. Qu, J.Y.; Wing, P.; Huang, Z.; Kwong, D.; Sham, J.; Lee, S.L.; Ho, W.K.; Wei, W.I. Preliminary study of in vivo autofluorescence of nasopharyngeal carcinoma and normal tissue. *Lasers Surg. Med.* **2000**, *26* (5), 432–440.
 58. Ramanujam, N.; Mitchell, M.F.; Mahadevan, A.; Thomsen, S.; Malpica, A.; Wright, T.; Atkinson, N.; Richards-Kortum, R. Development of a multivariate statistical algorithm to analyze human cervical tissue fluorescence spectra acquired in vivo. *Lasers Surg. Med.* **1996**, *19* (1), 46–62.
 59. Lin, W.; Yuan, X.; Yuen, P.; Wei, W.I.; Sham, J.; Shi, P.; Qu, J. Classification of in vivo autofluorescence spectra using support vector machines. *J. Biomed. Opt.* **2004**, *9* (1), 180–186.
 60. Zangaro, R.A.; Silveira, L.J.; Manoharan, R.; Zonios, G.; Itzkan, I.; Dasari, R.R.; Van Dam, J.; Feld, M.S. Rapid multiexcitation fluorescence spectroscopy system for in vivo tissue diagnosis. *Appl. Opt.* **1996**, *35* (25), 5211–5219.
 61. Ramanujam, N.; Mitchell, M.F.; Mahadevan, A.; Warren, S.; Thomsen, S.; Silva, E.; Richards-Kortum, R. In vivo diagnosis of cervical intraepithelial neoplasia using 337-nm-excited laser-induced fluorescence. *Proc. Natl. Acad. Sci. USA* **1994**, *91* (21), 10193–10197.
 62. Nath, A.; Rivoire, K.; Chang, S.; West, L.; Cantor, S.B.; Basen-Engquist, K.; Adler-Storthz, K.; Cox, D.D.; Atkinson, E.N.; Staerkel, G.; MacAulay, C.; Richards-Kortum, R.; Follen, M. A pilot study for a screening trial of cervical fluorescence spectroscopy. *Int. J. Gynecol. Cancer* **2004**, *14* (6), 1097–1107.
 63. Brewer, M.; Utzinger, U.; Silva, E.; Gershenson, D.; Bast, R.C., Jr.; Follen, M.; Richards-Kortum, R. Fluorescence spectroscopy for in vivo characterization of ovarian tissue. *Lasers Surg. Med.* **2001**, *29* (2), 128–135.
 64. Tadrous, P.J.; Siegel, J.; French, P.M.; Shousha, S.; Lalani, el N.; Stamp, G.W. Fluorescence lifetime imaging of unstained tissues: early results in human breast cancer. *J. Pathol.* **2003**, *199* (3), 309–317.
 65. Neerken, S.; Lucassen, G.W.; Bisschop, M.A.; Lenderink, E.; Nuijs, T.A. Characterization of age-related effects in human skin: a comparative study that applies confocal laser scanning microscopy and optical coherence tomography. *J. Biomed. Opt.* **2004**, *9* (2), 274–281.
 66. Rajadhyaksha, M.; Gonzalez, S.; Zavislan, J.M.; Anderson, R.R.; Webb, R.H. In vivo confocal scanning laser microscopy of human skin II: advances in instrumentation and comparison with histology. *J. Invest. Dermatol.* **1999**, *113* (3), 293–303.
 67. Hanlon, E.B.; Manoharan, R.; Koo, T.W.; Shafer, K.E.; Motz, J.T.; Fitzmaurice, M.; Kramer, J.R.; Itzkan, I.; Dasari, R.R.; Feld, M.S. Prospects for in vivo Raman spectroscopy. *Phys. Med. Biol.* **2000**, *45* (2), R1–59.
 68. Skala, M.C.; Squirrell, J.M.; Vrotsos, K.M.; Eickhoff, J.C.; Gendron-Fitzpatrick, A.; Eliceiri, K.W.; Ramanujam, N. Multiphoton microscopy of endogenous fluorescence differentiates normal, precancerous, and cancerous squamous epithelial tissues. *Cancer Res.* **2005**, *65* (4), 1180–1186.
 69. Yasui, T.; Tohno, Y.; Araki, T. Characterization of collagen orientation in human dermis by two-dimensional second-harmonic-generation polarimetry. *J. Biomed. Opt.* **2004**, *9* (2), 259–264.